ChemPubSoc Europe

DOI: 10.1002/slct.201803417

Chemistry SELECT Full Papers

Energy Technology & Environmental Science

Sweet-Lime-Peels-Derived Activated-Carbon-Based Electrode for Highly Efficient Supercapacitor and Flow-Through Water Desalination

Dinesh J. Ahirrao,[a] Sneha Tambat,[b] A. B. Pandit,[b] and Neetu Jha*[a]

In the present work, highly porous activated carbon with an excellent surface area has been successfully synthesized from the agricultural waste product; sweet lime peels (Citrus limetta) using a facile chemical approach. The structural and morphological properties of sweet lime peels derived activated carbon (SLP-AC) were studied using X-ray diffraction (XRD), Raman spectroscopy, scanning electron microscopy (SEM), and X-ray photoelectron spectroscopy (XPS). Brunauer-Emmett-Teller (BET) surface area and pore structure were studied using nitrogen adsorption-desorption isotherms. Electrochemical characterizations were performed in two and three electrode cell configurations using techniques like cyclic voltammetry (CV), Galvanostatic charge-discharge (GCD) and electrochemical impedance spectroscopy (EIS) in aqueous (1 M H_2SO_4 and 1 M NaCl) and ionic liquid electrolytes ($EMIMBF_4$). SLP-AC based electrodes showed high electrochemical charge storage capacity of 421.67 F/g (at 1 A/g) along with outstanding cyclic stability up to 10000 GCD cycles. Fabricated supercapacitor device demonstrated high energy density of 45.53 Wh/kg in the ionic liquid electrolyte. SLP-AC was also used to prepare the porous sponge electrodes to study their applicability in flow-through electrode capacitive deionization (CDI), where it achieved the maximum electrosorption capacity of 22.8 mg/g. The electrosorption results fitted well with the Langmuir isotherm and the kinetics study indicates a pseudo-first-order kinetic model for the electrosorption of salt ions onto the electrodes surface. This confirms the outstanding performance of SLP-AC as a highly stable and low-cost electrode material for supercapacitors and water desalination applications.

Introduction

Waste management is a global issue, which needs immediate attention to evade further consequences. In India, per capita waste generation, in cities is in the range of 200 to 600 grams per day. With the alarming increase in population growth, this rate of waste production will continue to increase. According to the report provided by the ministry of environment and forest, in the year 2016, India alone is responsible for the production of 62 million tons of waste per annum. Out of this, only 75–80% of the waste gets collected and 22–28% of it is recycled in an environmentally friendly way and rest is allowed to lie in the landfills and forests. The ministry estimated that by the year 2030, waste generation will increase from 62 million tons to about 165 million tons per year. It is an inevitable desire of humankind to get rid of the waste but practically it is very difficult to completely dispose of such a tremendous amount of waste. This is one of the most serious threats to mankind, which needs to be resolved at priority.

Majority of waste that is being generated can possibly be the potential precursor for the production of carbon.[1] However, the sum of waste accrues only from the sweet lime is worth noticing, because its production is about 15% per year of a total fruit market and it is one of the most cultivated fruit worldwide.[2] Citrus fruits waste is considered unsafe and has the potential to cause soil pollution if directly deposed into the soil because it releases phenol compounds which decreases the soil fertility.[3] The sweet lime peels are composed of cellulose, hemicelluloses, and pectin. These are well known and excellent natural precursors for the production of carbon.[4] Hence, to avoid its unwanted effects on soil, it is better to process it for the production of high surface area activated carbon for its various promising carbon-based applications like energy storage and desalination.

Energy storage devices like supercapacitors (SCs) have gained huge attention in recent times due to their fascinating features like high power density, excellent cycling stability, and high durability.[5] Supercapacitors can be used in the wide range of applications where short-term energy burst is required such as; electric vehicles, power tools, hybrid cars, trains, and buses for the regenerative braking system. Supercapacitors are categorised into two types based on their charge storage mechanisms; pseudocapacitors and electric double layer capacitors (EDLCs). In pseudocapacitors, electrodes are fabricated using a metal oxide or conducting polymer, which stores the charges by means of redox reactions (faradically). Unfortunately, the practical use of pseudocapacitors is restricted owing

[a] D. J. Ahirrao, Dr. N. Jha
Department of physics, Department of chemical engineering, Institute Of Chemical Technology, Mumbai-400019, India
E-mail: nr.jha@ictmumbai.edu.in
[b] S. Tambat, Prof. A. B. Pandit
Department of chemical engineering, Institute Of Chemical Technology, Mumbai-400019, India
E-mail: nr.jha@ictmumbai.edu.in

Supporting information for this article is available on the WWW under https://doi.org/10.1002/slct.201803417

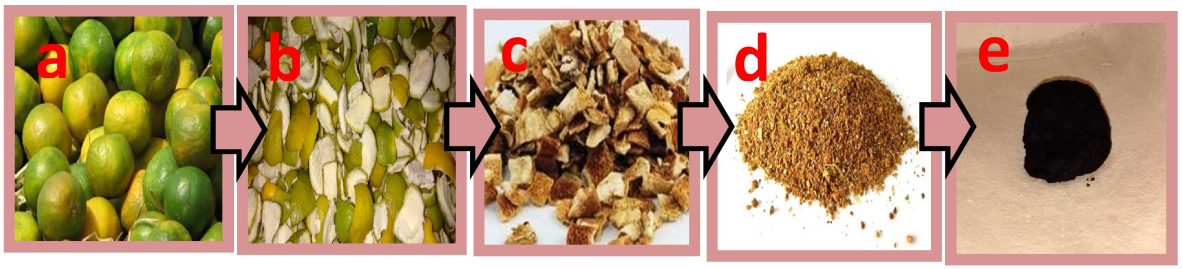

Figure 1. Optical images for the synthesis procedure of SLP-AC (a) Sweet lime (b) Sweet lime peels (c) Dried sweet lime peels (d) Grinded peels (e) SLP-AC after carbonization.

to their low cyclic stability and poor electrical conductivity.[6] On the other hand, EDLCs employs carbon nanomaterials with high surface area and excellent electrical conductivity to store the charges electrostatically at the electrode-electrolyte interface (Non-faradically). Lately, the use of carbon materials derived from waste or biomass has become fascinating for various applications, especially for energy storage due to the continuous decrease in the availability of fossil fuels.[7,8] It has been reported by number of researchers that high surface area activated carbon with excellent energy storage capabilities can be prepared from various sources like; cow dung,[9] lotus pollen,[10] sunflower seeds,[11] silk,[12] protein,[13] soya bean,[14] watermelon,[15] hemp,[16] oil palm,[17] yogurt,[18] eggshell membrane,[19] coffee beans,[20] human hairs,[6] etc. Most of these materials are uncommon and difficult to find. Therefore, it would be appreciable and more practical if activated carbon can be prepared from cheap, plentiful but discarded natural wastes like sweet lime peels.

Water is considered as life for all living beings but its unplanned usage and exploitation of available freshwater resources, increasing population, and rapid growth of industries are the main culprits behind the scarcity of fresh water. This could be the cause of major concern in near future. Treating seawater or brackish water using desalination techniques can resolve this issue. The existing desalination technologies like reverse osmosis, membrane separation, electrodialysis etc. are already accessible but have some disadvantages like high energy consumption and requires regular maintenance.[21] Therefore, a cheap, reliable, and efficient desalination route needs to be investigated. In recent times, desalination by capacitive deionization (CDI) has attracted much interest due to its low cost, less energy requirement, and environmental compatibility.[22] CDI works on the principle of electric double layer capacitors (EDLCs). Where, the potential difference is applied across the pair of carbon-based electrodes, which forms an electric double layer at the electrode-electrolyte interface and separates the salt ions by accumulating them on to the oppositely charged electrodes. When the entire surface area of the electrodes gets saturated by adsorbing the ions; a reverse potential can be applied to regenerate the electrodes.[23] Carbon-based electrodes currently used in CDI or in supercapacitors are made up of the materials like amorphous carbon, graphene, and carbon nanotubes. These materials are either expensive, challenging to synthesize, or requires advanced facilities like chemical vapor deposition, laser ablation, sputtering, arc discharge, and others.[6] Therefore, a simple, environmentally friendly and cost-effective approach for the production of activated carbon encourages the advancement in biomass-derived carbon materials.

In this present work, we demonstrated a facile technique for the synthesis of highly porous activated carbon from waste sweet lime peels. Obtained sweet lime peels derived activated carbon (SLP-AC) was used for the fabrication of supercapacitor electrodes in order to study their electrochemical properties for energy storage applications. The energy storage capacity of SLP-AC electrodes were evaluated in aqueous and ionic liquid electrolytes at various scan rates and current densities. The cyclic stability test was carried out by performing 10000 continuous GCD cycles at 10 A/g of current density. Another set of electrodes was also prepared using the domestic sponge as a scaffold to evaluate the water desalination capabilities of SLP-AC in flow-through electrode capacitive deionization (CDI) cell. CDI tests were carried out using several NaCl concentrations (300 mg/L, 600 mg/L, and 900 mg/L) and at various applied voltages (0.8 V, 1 V, 1.2 V, and 1.4 V). Dissimilarity in the electrosorption was observed with the change in initial salt solution concentration and applied potential.

Results and discussion

Herein, we prepared the activated carbon from waste sweet lime peels at low tempreture using KOH activation (Figure 1). The structure and purity of as synthesized SLP-AC was examined using XRD. An XRD spectrum for SLP-AC consists of two broad peaks at $2\theta = 27.13°$ and $2\theta = 43.8°$ (Figure 2a), which corresponds to the reflections from the planes (002) and (100) respectively. This is the representation of the graphitic nature of SLP-AC.[25] The nature of the material was further explored by Raman spectroscopy. Figure 2b shows the Raman spectra for the SLP-AC. Raman spectra provide information about the molecular vibration and also determines the nature of the sample. It is widely used to describe the structural features of carbonaceous materials.[26,27] The peaks present at 1350 cm^{-1} and 1598 cm^{-1} correspond to the characteristic D and G bands of carbon respectively. The D band is associated with the defects, while G band corresponds to the vibration of

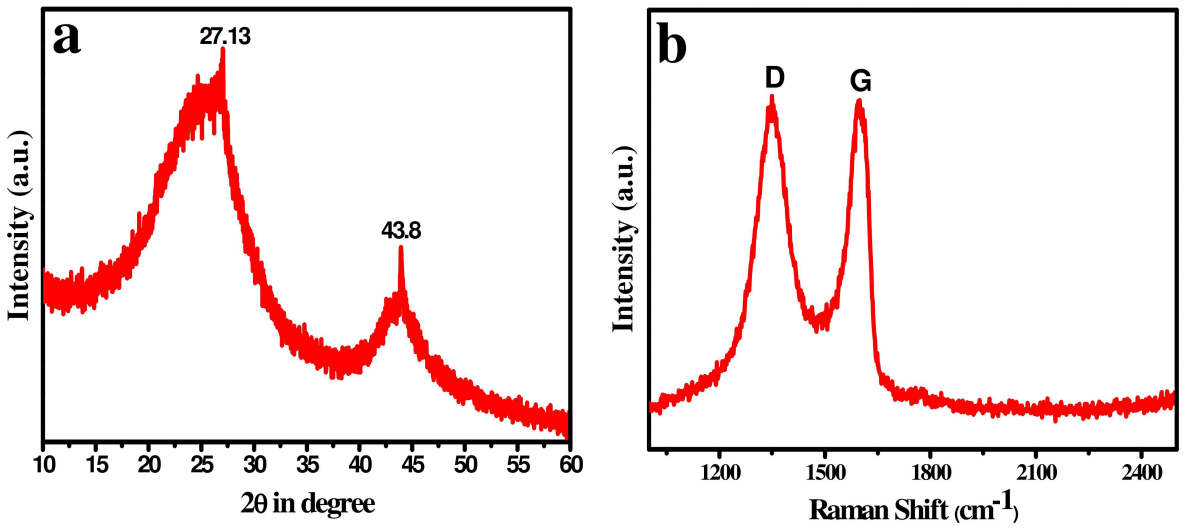

Figure 2. (a) X-ray diffraction pattern and (b) Raman spectrum for SLP-AC.

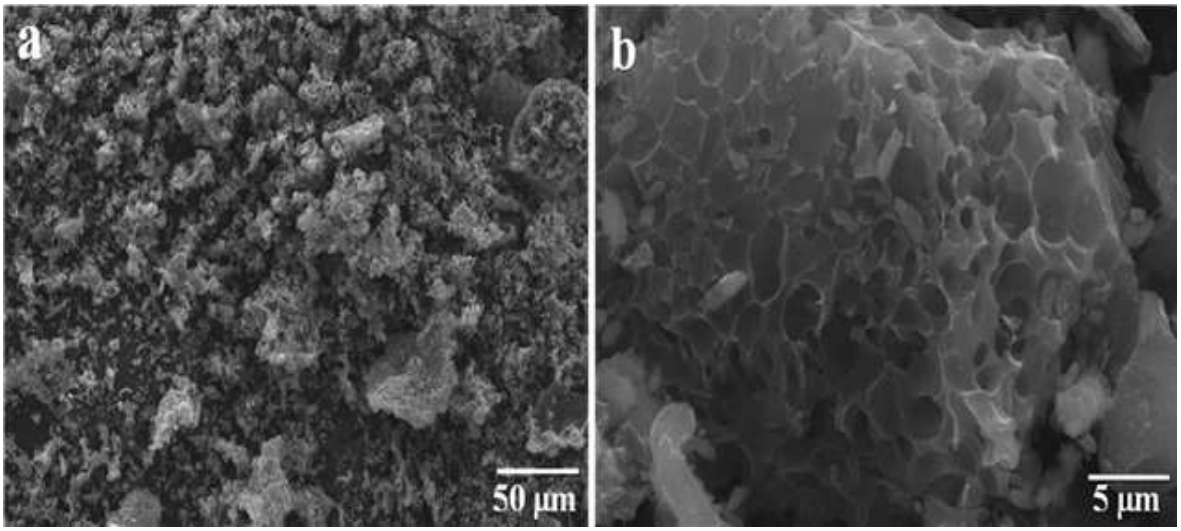

Figure 3. SEM images for SLP-AC at different magnifications.

sp^2 bonded atoms in a two-dimensional hexagonal lattice. The I_D/I_G ratio is significantly high (1.18), which indicates the existence of a disordered carbon matrix.[28]

Morphology and surface structure of as-prepared SLP-AC was examined by scanning electron microscope, as shown in Figure 3a and b. A highly porous spongy surface of SLP-AC is clearly visible in SEM micrographs at different magnifications. The material shows desired surface properties and micrometer size pores in both the SEM images. It confirms the efficient activation of carbon with KOH even at low temperature with the possibility of scale up.

An X-ray photoelectron spectroscopy (XPS) was performed to gather the information about elemental composition and nature of functional groups presents in SLP-AC. Survey scan (0-800 eV) in Figure 4a shows the existence of two prominent peaks for carbon (C1s) and oxygen (O1s) at 284.19 eV and 531.72 eV respectively. Exclusive presence of C1s and O1s peaks signifies the excellent purity of SLP-AC. The atomic percent obtained for carbon and oxygen is 90.52% and 9.48% respectively; with the C/O ratio of 9.54. High-resolution spectra for C1s was deconvoluted into four peaks including two major peaks for sp^2-hybridized C=C graphitic carbon at 284.19 eV and sp^3 hybridized C–C at 285.25 eV (Figure. 4b).[29] Remaining two peaks at 288.38 eV and 290.16 eV can be ascribed to -COOH[30] and O-C=O[31] respectively. Figure 4c shows the O1s spectra with the couple of de-convoluted peaks, which reveals the existence of a different kind of oxygen functionalities. The peak at 530.72 eV can be assigned to C–O, C=O (carbonyl), COOH (carboxyl) groups. Whereas, the peak at 532.36 contributes to the epoxy (C–O) group.[32,33]

Wettability of the material is a decisive factor for desalination application. Here, we carried out the water contact angle

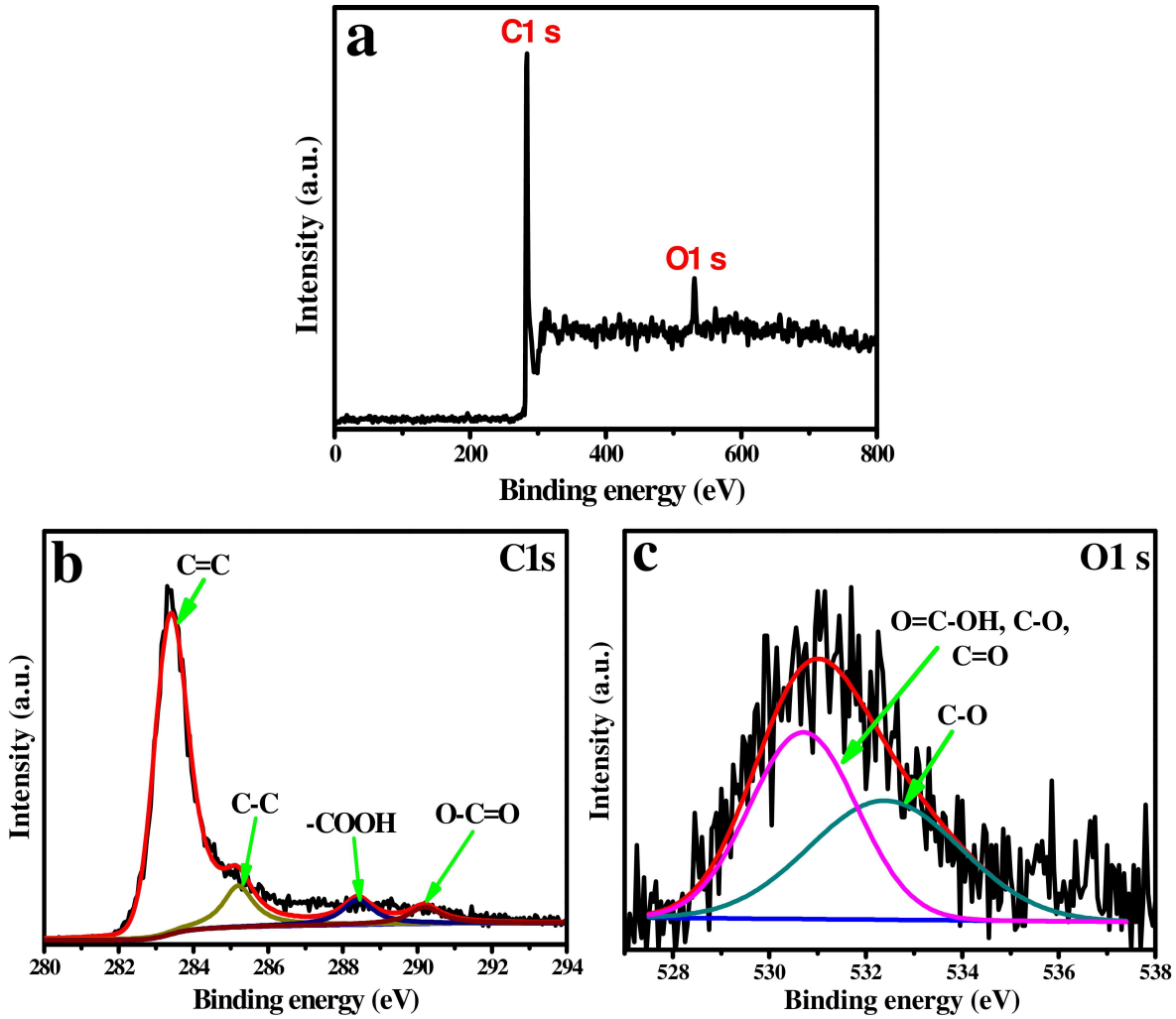

Figure 4. XPS spectra of SLP-AC (a) Survey scan; High-resolution scan for (b) Carbon C1s (c) Oxygen O1s.

(WCA) test to determine the contact angle of as prepared SLP-AC (Figure 5). Interestingly, the presence of the oxygen-containing functional group in SLP-AC has significantly reduced its contact angle to 22° thus demonstrating excellent penetration of water droplet within the sample without any restraint. The reason behind its outstanding wettability is not only the presence of oxygenated functional groups but also its porous framework. Furthermore, employing this kind of hydrophilic material with superior wettability as a CDI electrode is expected to enhance the electrosorption performance.

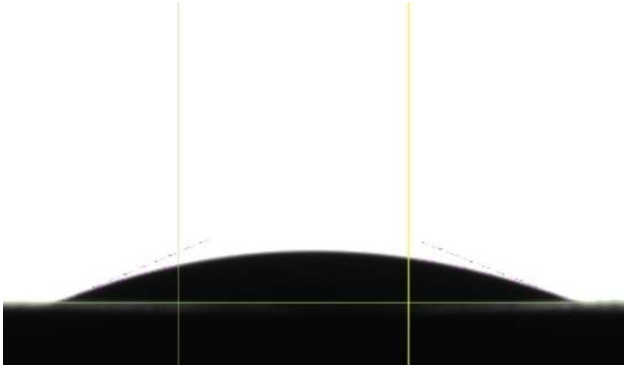

Figure 5. Contact angle determination of a water droplet on SLP-AC surface.

The BET surface area and pore size distribution for SLP-AC are shown in Figure 6a and b. The measurements were carried out by Brunauer-Emmett-Teller (BET) using nitrogen adsorption-desorption isotherm. The obtained BET surface area for SLP-AC is 667.87 m^2/g with the total pore volume of 0.1437 cc/g. The nature of adsorption curve perfectly fits for type-I isotherm; which represents the microporous material.[34] The slope appears at a lower relative pressure in between 0.4-0.8, confirms the existence of mesopores and at higher relative pressure 0.8-1.0 is ascribed to macropores.[35] Figure 6b shows the pore size distribution plot which was obtained by the Barret-Joyner-Halenda (BJH) method. It can clearly be observed

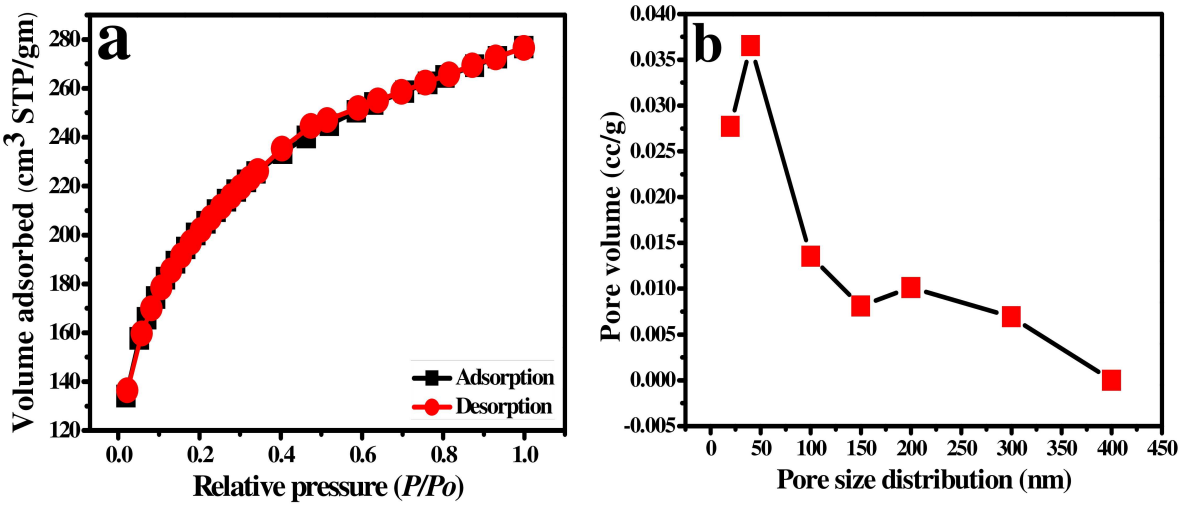

Figure 6. BET surface area determination of SLP-AC (a) N_2 adsorption-desorption isotherm and (b) Pore size distribution.

that the maximum pores are in the range of 15 to 400 nm and most of the pores are having a diameter of 50 nm. The interconnected macropores present inside the SLP-AC network allows buffering of ions and reduces the diffusion space from the electrolyte to the inner surfaces of SLP-AC[36] and the mesopores on thin walls improve the ionic movement and electrosorption capacity.[37]

Electrochemical characterizations

Electrode preparations for three-electrode cell

To study the electrochemical behavior of SLP-AC in three-electrode cell configuration; glassy carbon (GCE) was used as a working electrode along with the counter (platinum wire) and a reference electrode (Ag/AgCl). To prepare the electrode, SLP-AC (10 mg) was added into the solution mixture of DI water (1 mL) and ethanol (1 mL) followed by 2 hour of sonication. Obtained homogeneous suspension of electro-active material (5 µl) was drop cast on to a 3 mm diameter GCE. Total calculated mass loading on GCE was 25 µg (0.35 mg/cm^2). Electrochemical tests like CV and GCD were performed in the potential window of 0 to 0.9 V using 1 M H_2SO_4 electrolyte solution. Specific capacitance was calculated from the GCD curves using following formula (1).[38]

$$SC\left(\frac{F}{g}\right) = \frac{I \times \Delta t}{m \times \Delta V} \quad (1)$$

Where, SC is the specific capacitance (F/g), I represents the applied current (A), Δt is the discharge time (s), m is the mass of electrode (g) and ΔV is the potential window (V).

Electrochemical measurements using three-electrode cell

Electrochemical analysis plays an important role in order to study the complete electrochemical response of the electrode material including the charge holding capacity and charge storage behavior.

High porosity and improved surface area of SLP-AC is expected to demonstrate the superior capacitive performance. To study the energy storage capabilities of as prepared SLP-AC; the electrochemical tests were precisely studied in the three-electrode system using 1M H_2SO_4 electrolyte. Figure 7a shows the cyclic voltammetry curves at scan rates ranging from 50 to 350mV/s. The increase in current response with scan rates is clearly visible in all CV curves along with its electric double layer (EDL) behavior coupled with some contribution of pseudocapacitance; which must be caused by the presence of oxygen-containing functional groups in SLP-AC as evident from the XPS spectra.[11,15]

Figure 7b shows the galvanostatic charge-discharge curves at current densities ranging from 1 to 3.5A/g. The GCD curves are almost triangular in shape except the little hump at the end of the discharging curve again validating the influence of pseudocapacitance. However, the IR drop in all GCD curves is very less, thus representing the good energy storage behavior of SLP-AC. The specific capacitance values determined using equation (1) are 421.67, 383.57, 377.45, 375.05, 373.52 and 372.61 F/g at the current densities of 1, 1.5, 2, 2.5, 3 and 3.5 A/g respectively. Figure 7c corresponds to the specific capacitance versus current density plot confirming the typical behavior of supercapacitor, where specific capacitance decreases with increasing current densities. This happens due to the reduced penetration of electrolyte ions into the pores of the electrode material at higher current densities. The high values of specific capacitances obtained here are due to the higher surface area and optimum pore structure of as-synthesized material.[20]

Electrode preparations for symmetric two-electrode cell

To investigate the electrochemical properties of SLP-AC in symmetric two electrode cell; initially, electrodes were prepared by making suspension of 50 mg of electro-active material (SLP-

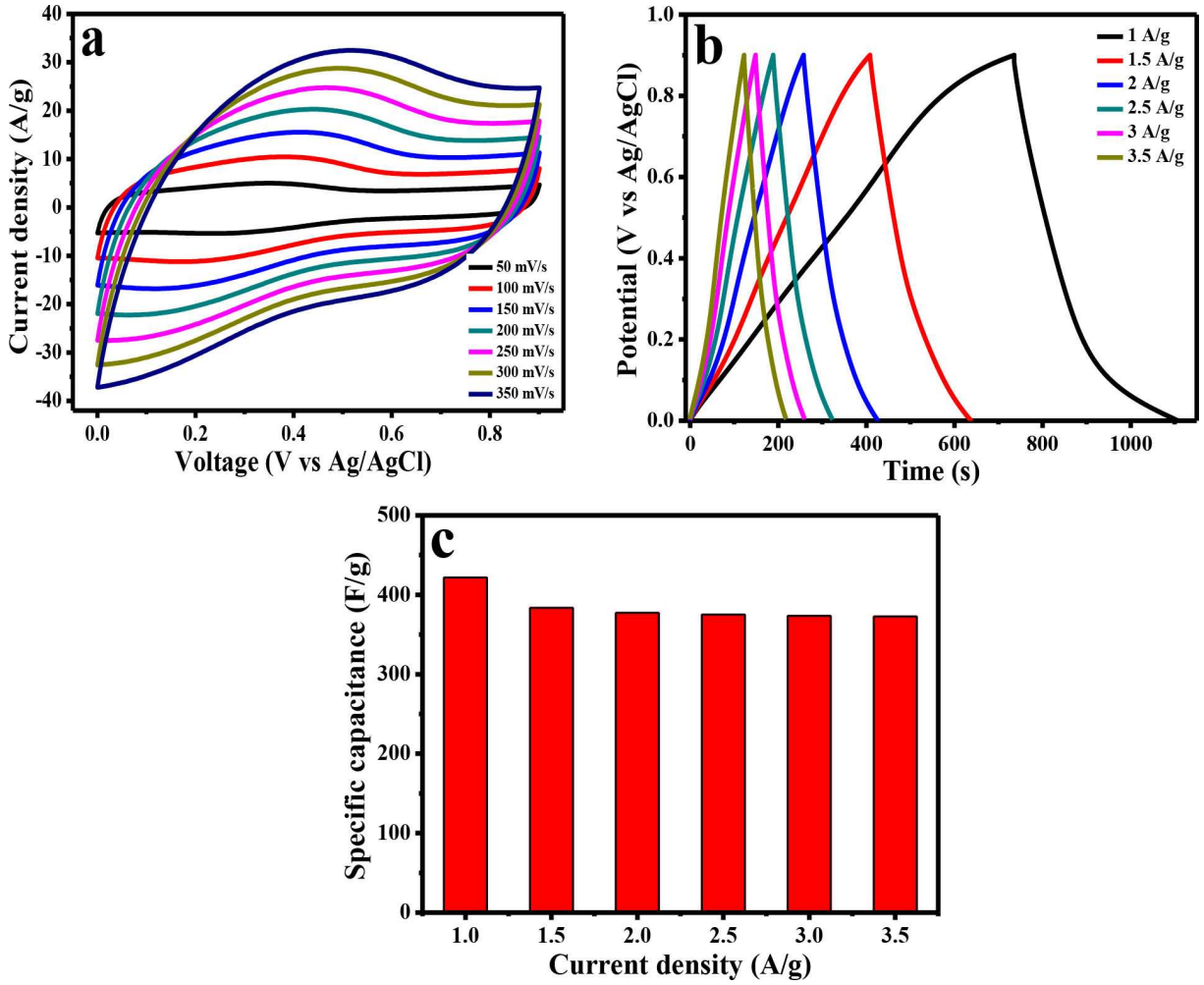

Figure 7. Electrochemical analysis for SLP-AC using three-electrode cell configuration (in 1 M H_2SO_4 electrolyte) (a) Cyclic voltammetry at scan rates from 50 to 350 mV/s (b) Galvanostatic charge-discharge at current densities from 1 to 3.5 A/g (c) Specific capacitance versus current density plot.

AC) in the solution of ethanol (2 mL) and DI water (2 mL) followed by 2 hours of sonication in a bath sonicator. As prepared SLP-AC ink was spin coated on to the graphitic carbon paper and dried for 2 hours at room temperature. Amount of loading was measured gravimetrically by weighing the graphitic carbon paper before and after the coating. Three pair of electrodes were prepared with mass loading of 6 mg (3.82 mg/cm^2), 3 mg (1.91 mg/cm^2), and 5.2 mg (3.31 mg/cm^2) for the analysis in 1 M H_2SO_4, 1 M NaCl, and $EMIMBF_4$ electrolytes respectively. Swagelok cell assembly was used to fabricate the symmetric two electrode supercapacitor. Whatman filter paper soaked with an electrolyte was used as a separator between the electrodes. Electrochemical studies like GCD was performed at current densities ranging from 1 to 3.5 A/g and CV was performed at the scan rates ranging from 50 to 350 mV/s. EIS was recorded in the frequency range from 100 kHz to 0.01 Hz. Electrochemical data were collected in the potential window of 0 to 0.9 V with aqueouselectrolyte solutions. To evaluate the energy density and power density of SLP-AC electrodes, the electrochemical response was recorded in the ionic liquid electrolyte at a higher potential window of 0 to 3 V. Following equations were used to calculate the specific capacitance (C_s), energy density (E) and power density (P).[38]

$$C_m = \frac{I}{m \times \frac{dv}{dt}} \tag{2}$$

$$C_s = 4 \times C_m \tag{3}$$

Where, C_m (F/g) is the capacitance of the device, I (A) is the current, m (mg) is total mass of electro-active material loaded on both the electrodes, dt (s) and dV (V) are the discharge time and potential window respectively.

$$E = \frac{\frac{1}{2} CV^2}{3.6} \tag{4}$$

$$P = \frac{E \times 3600}{\Delta t} \tag{5}$$

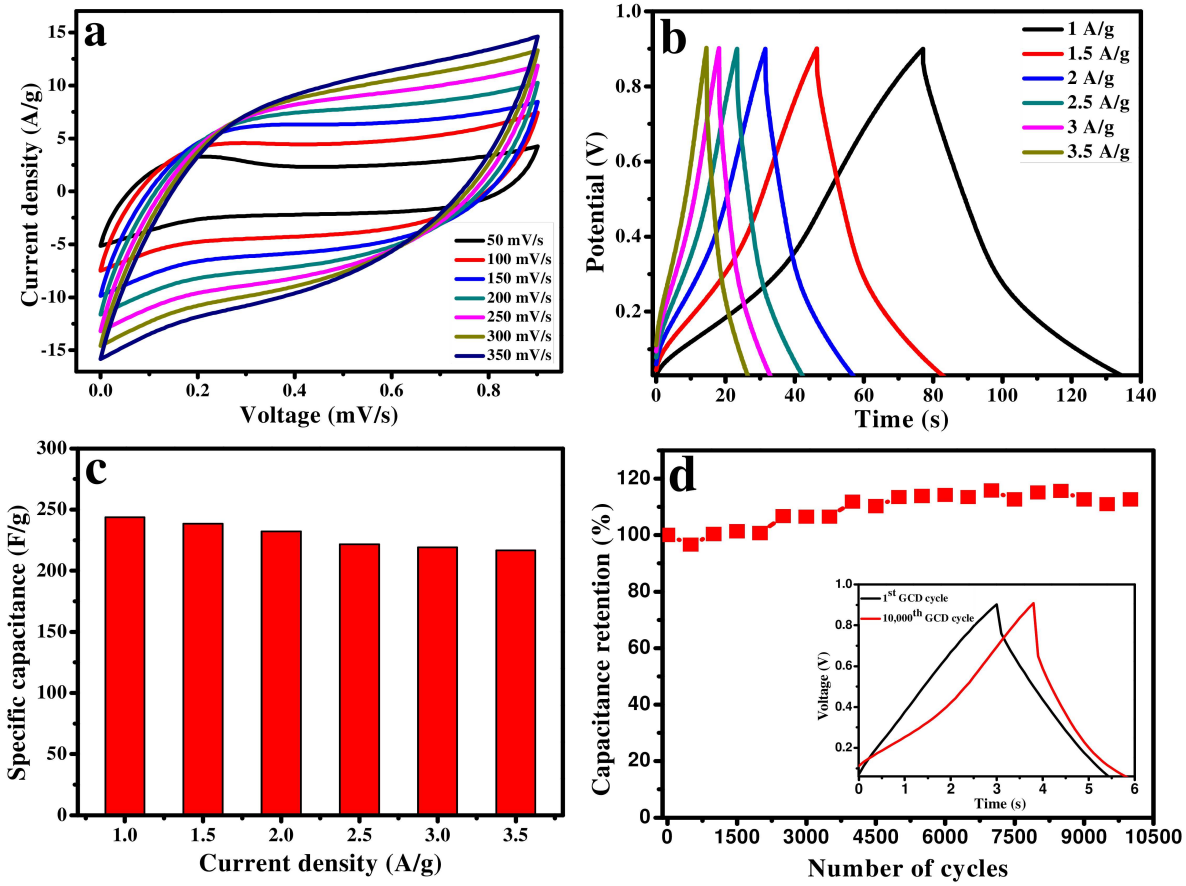

Figure 8. Electrochemical analysis for SLP-AC using two-electrode symmetric cell configuration (in 1 M H_2SO_4 electrolyte) (a) Cyclic voltammetry at scan rates from 50 to 350 mV/s (b) Galvanostatic charge-discharge at current densities from 1 to 3.5 A/g (c) Specific capacitance versus current density plot (d) cyclic stability test up to 10000 GCD cycles (at 10 A/g).

Where, V (Volt) is the working potential window and t (s) is the time required to discharge the cell.

Electrochemical measurements using two-electrode cell

Figure 8a shows the cyclic voltammetry measurements for SLP-AC electrodes recorded at various scan rates. All the CV curves have maintained their shape even at the higher scan rates without showing any distortion; suggesting a good electrochemical response of SLP-AC. The charge storage mechanism of SLP-AC is due to the amalgamation of an electric double layer and pseudocapacitance. That means there are some oxidation and reduction reactions are taking place at the electrode-electrolyte interface. The combination of EDL and redox behavior can clearly be understood from the partially rectangular shape of CV curves. To confirm the redox contribution in SLP-AC electrodes; cyclic voltammetry tests were also carried out at lower scan rates starting from 5 mV/s to 45 mV/s (Figure S1b in the supporting information). From all the CV data it is clear that no prominent faradic peaks are visible. However, the shape of the CV curves is not perfectly rectangular either, demonstrating the electric double layer dominating the charge storage processes.

Further to calculate the specific capacitance of SLP-AC, electrodes were subjected to GCD studies at the range of current densities as shown in Figure 8b. The GCD curves represent the distinctive symmetric shape with small platues at the end of charging and discharging curves, demonstrating the little influence of pseudocapacitance. The specific capacitance values calculated from the GCD curves using equations (2) and (3) are 295.45, 286.19, 272.52, 260.74, 249.71, and 240.2 F/g at the current densities of 1, 1.5, 2, 2.5, 3, and 3.5 A/g respectively. Figure 8c verifies the characteristic behavior of supercapacitor, where energy storage capacity reduces with increasing current densities. The capacitance of the sample showed 48.31% retention when we increased the current density from 1 to 25 A/g (Figure S1c in the supporting information). This indicates an excellent rate capability of SLP-AC electrode. For the comparison purpose, electrochemical performance of the graphitic carbon paper was also studied in 1 M H_2SO_4 electrolyte. It exhibited a nominal specific capacitance of 7.99 F/g at 1 A/g of current density (Figure S1a in the supporting information).

Another important parameter to evaluate the supercapacitors performance is their cyclic stability. It measures the ability of electrode material to sustain continuous charging-discharg-

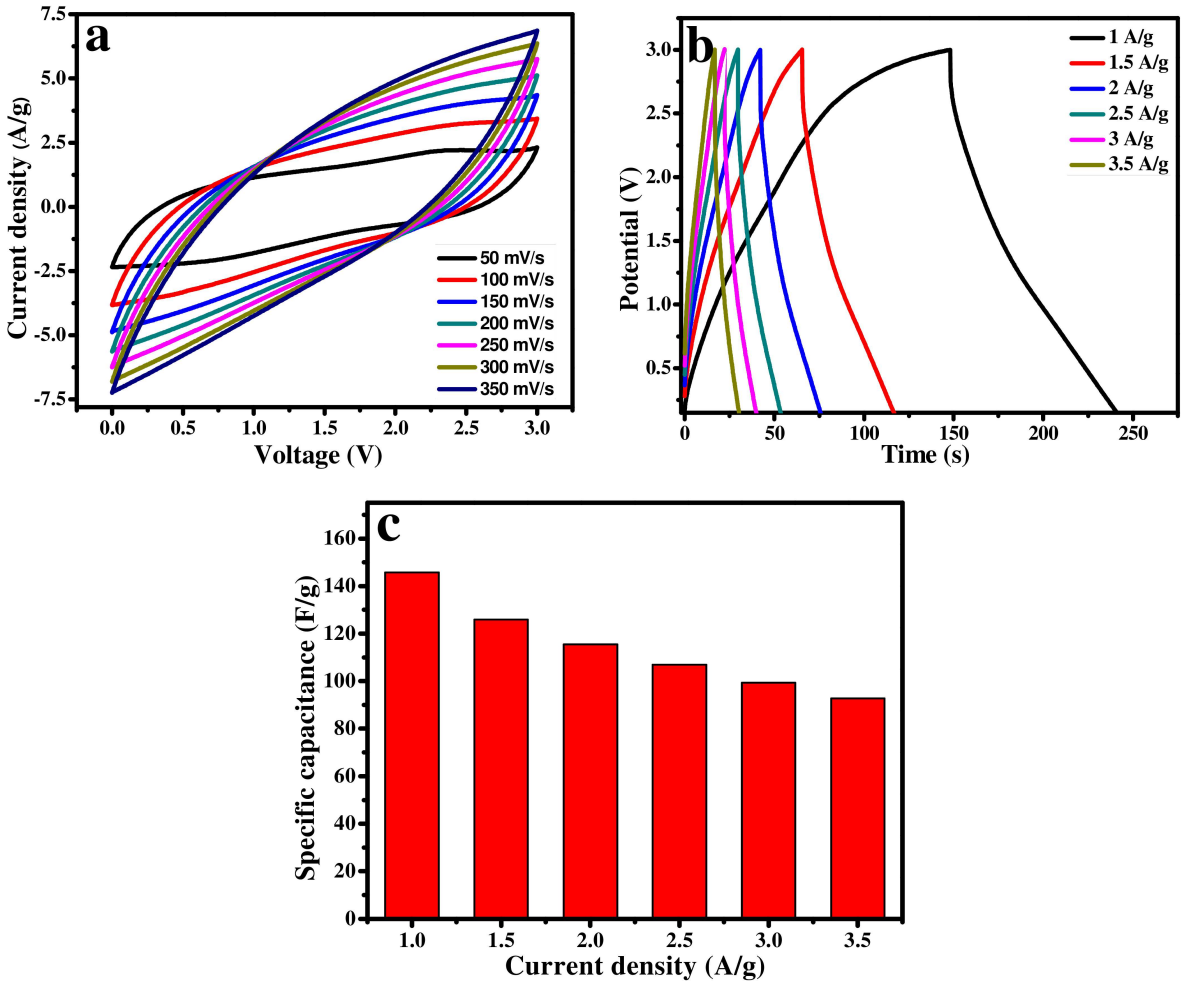

Figure 9. Electrochemical analysis for SLP-AC using two-electrode symmetric cell configuration in ionic liquid electrolyte ($EMIMBF_4$) (a) Cyclic voltammetry at scan rates from 50 to 350 mV/s (b) Galvanostatic charge-discharge at the current densities from 1 to 3.5 A/g (c) Specific capacitance versus current density plot.

ing cycles for a long period of time and its effects on the overall performance of the supercapacitor. Cyclic stability results also help to understand the durability and efficiency of the electrode material. Here we performed a cyclic stability test for 10000 charge-discharge cycles at the current density of 10 A/g (Figure 8d). No fading in specific capacitance was observed after the stability test instead the charge holding capacity has increased by 12%. This is due to the electro-activation of the electrode material. Electro-activation is a fascinating phenomenon in which the charge holding capacity of the electrodes increases with the number of charging-discharging cycles. It is anticipated that in electro-activation the layers of electrode material start to move with the increasing charge-discharge cycles to accommodate the maximum electrolyte ions. Therefore, ions gets access to the maximum surface area of the electrodes and intercalate into the pores of the material; which results in increasing the charge holding capacity of the electrode material.[39]

Though the aqueous electrolytes are cheap, chemically stable, and easy to handle; There are certain limitations that are associated with them; they can only work in a limited potential window and temperature range ($<$ 1.23 volt).[20] Hence, it is very demanding to fabricate the high energy density energy storage devices. In order to achieve the maximum energy density; electrodes should be analyzed in ionic liquid electrolyte due to their wide working potential window. We therefore thoroughly investigated the electrochemical performance of the SLP-AC electrodes in an ionic liquid electrolyte ($EMIMBF_4$). The electrochemical analysis was carried out in the potential window of 0–3 V. Equations (4) and (5) was used to calculate the energy density and power density respectively. CV plots (Figure 9a) for SLP-AC continues to demonstrate the same charge storage mechanism as explained earlier, by validating the little faradic involvement along with the electric double layer. Figure 9b shows the GCD curves in the higher potential window. The specific capacitance values obtained (Figure 9c) from SLP-AC electrodes in an ionic liquid electrolyte are 145.7, 125.86, 115.48, 106.88, 99.32, and 97.71 F/g at the current densities of 1, 1.5, 2, 2.5, 3, and 3.5 A/g respectively. These values of specific capacitance are less when compared with the values obtained from the aqueous electrolyte. This can be attributed to the higher viscosity of ionic liquid electrolyte,

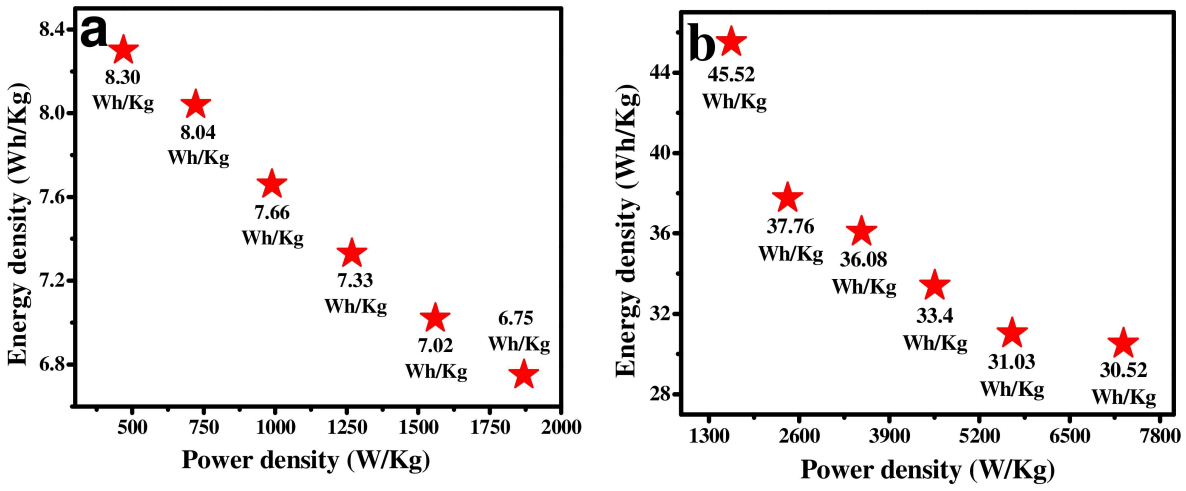

Figure 10. Energy density versus power density (Ragone plot) (a) In aqueous electrolyte (1 M H_2SO_4) (b) In ionic liquid electrolyte ($EMIMBF_4$).

which reduced the mobility of the electrolyte ions inside the electrode volume.[40,41]

The performance of SLP-AC was further evaluated with the Ragone plot (Figure 10a and b). Generally, the increase in power density leads to a reduction in energy density.[42] We noticed similar behavior with SLP-AC, but surprisingly no considerable reduction in energy density was observed with increasing power density. This reveals the stable and superior performance of SLP-AC electrodes. In most of the reports it has also been observed that the energy density also decreases with increasing current density. Because, at the higher current densities only surface pores are accessible to the electrolyte ions, which causes rapid charging and discharging of the supercapacitor cell. Whereas, at lower current density almost every pore is approachable to electrolyte ions, whether it is at surface or in the inner depth of the electrode, hence the supercapacitor discharges slowly.[43] However, for SLP-AC electrodes, even with the increasing current density there was not much decrease in energy density value was observed (8.30 Wh/kg at 1 A/g to 6.75 Wh/kg at 3.5 A/g in aqueous electrolyte and 45.52 Wh/kg at 1 A/g to 30.52 Wh/kg at 3.5 A/g in ionic electrolyte).

EIS is a powerful tool to scrutinize the electrode-electrolyte response towards the wide frequency range. It also helps to understand the internal resistance of the electrode material and the resistance between the electrode-electrolyte interface. Hence, EIS was performed to analyze the detailed electrochemical performance of the SLP-AC electrodes with different electrolytes (1 M H_2SO_4 and in $EMIMBF_4$). Figure 11a show the Nyquist plot based equivalent circuit. Figure b and c displays the experimental and fitted EIS plots of SLP-AC electrodes. The Nyquist plot consists of initial intercept at real axis followed by a semicircle and Warburg impedance, i.e. high frequency, mid frequency, and low-frequency regions respectively. The slight semicircle at high to mid-frequency region represents the poorer ion diffusion resistance and straight line at the low-frequency region specifies an ideal capacitive behavior, which

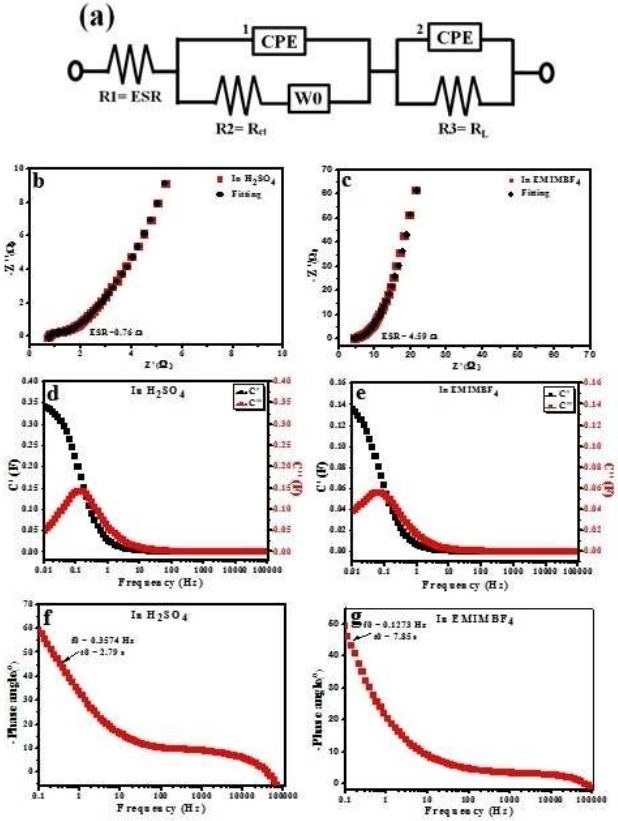

Figure 11. Electrochemical impedance spectroscopy of SLP-AC in aqueous and ionic electrolytes (a) The equivalent circuit (b and c) Experimental and fitted Nyquist plot (d and e) Bode plot for real and imaginary capacitance (f and g) Bode plot versus frequency plot.

was also confirmed from the CV and GCD curves (Figure 8a and b, 9a and b). The equivalent circuit diagram obtained after simulating the experimental data includes the components like equivalent series resistance (ESR); ESR represents the overall cell resistance including electrolyte resistance, the resistance

between current collector-electrode and Ohmic resistance at the electrode-electrolyte interface. ESR for SLP-AC in 1 M H_2SO_4 is as low as, 0.76 Ω due to the low viscosity of aqueous electrolyte and highly porous and conductive nature of the electrode material, which allows rapid adsorption of electrolyte ions into the porous electrode surface. Whereas, in an $EMIMBF_4$, ESR has increased to 4.59 Ω. This can be attributed to high viscosity of ionic liquid electrolyte, which causes the resistance for ion adsorption on to the electrode surface. R2 is the charge transfer resistance (R_{CT}); it represents the resistance to charge transfer from electrolyte solution to electrode surface. Aqueous electrolyte studies exhibited R_{ct} of 0.33 Ω and in ionic liquid it reached upto 1.74 Ω. Low charge transfer resistance suggests fast ion transport within the supercapacitor and vice versa. Next, the constant phase element (CPE) is simply a parameter in which the circuit element is acting in between the capacitor and the resistor. CPE is the non-ideal capacitance of the diffusion layer with the degree of deviation α (α = 1 for perfect capacitive behavior and 0 for perfect resistive behavior), which is associated with the capacitance arises in the diffusion layer.[9] Here, CPE 1 representing the double layer capacitance (CPE_{DL}); which arises at the interfaces between solid and ionic solutions due to separation of ionic and/or electronic charges and CPE 2 denotes pseudocapacitance, which occurs with voltage dependent faradic charge transfer processes (CPE_L).[44] Warburg impedance (W) is the obstruction to diffusion of electrolyte ions through the porous structure of electrode material.[45] R_L is the leakage resistance which is kept parallel to CPE_L.

The complex capacitance $C(\omega)$, relies on the real part of cell capacitance (C') and the imaginary part (C''), which is related to losses of energy dissipation and frequency. Assessment of the complex capacitance is an outstanding way to get an insight of the bulk and interfacial properties of the supercapacitor. Frequency-dependent real (C') and imaginary (C'') capacitances are calculated using the equations (7) and (8) and plotted data are shown in Figure 11d and e.[46]

$$C(\omega) = C'(\omega) - jC''(\omega) \tag{6}$$

$$C' = \frac{-Z''(\omega)}{\omega|Z(\omega)|^2} \tag{7}$$

$$C'' = \frac{Z'(\omega)}{\omega|Z(\omega)|^2} \tag{8}$$

Where, $Z(\omega)$ is equal to $1/j(\omega)C(\omega)$, $Z'(\omega)$ is the real impedance and $Z''(\omega)$ is the imaginary impedance and $\omega = 2\pi f$ (f – frequency (Hz)).

Figure 11f and g show the Bode plots which help to determine the crucial parameter like relaxation time constant (τ_0) of the supercapacitor. The resistive and capacitive behavior of the supercapacitor is equal at a phase angle of −45°, and the frequency at this particular angle is called as the knee frequency (f_0). The obtained knee frequency (f_0) at a phase angle of −45° for SLP-AC in 1 M H_2SO_4 is 0.3574 Hz and in $EMIMBF_4$ is 0.1273 Hz; which corresponds to the relaxation time constant $\tau_o(1/f_0)$ of 2.79 s and 7.85 s, respectively. Low τ_o is the indication of higher power delivery performance of supercapacitor.

Fabrication of flow-through electrode CDI cell

Electrosorption properties of SLP-AC sponge electrodes were studied in a flow-through electrode CDI cell. The cell is made up of an acrylic casing with dimensions of 10 cm X 10 cm X 1.5 cm. To prevent the water pressure in the cell; both sides of acrylic casing were provided with the circular reservoirs along with small holes to fit the 2 mm valve for water inlet and outlet. The diameter of reservoirs was 5 cm and depth was 4 mm. Whatman filter paper was used as a separator between the electrodes. One side of both the electrode was kept in contact with the copper current collector. Copper sheets also have two holes to circulate the water. All the inlets and outlets provided in the cell for water circulation are positioned in such a way that it helps to expose the electrodes surface to saline water during the experiment. Electrodes, current collectors, and separator are sandwiched in an acrylic casing as shown in Figure 12a. The gaskets were also inserted in assembly to prevent the water leakage. Stainless steel bolts were used to seal the entire assembly.

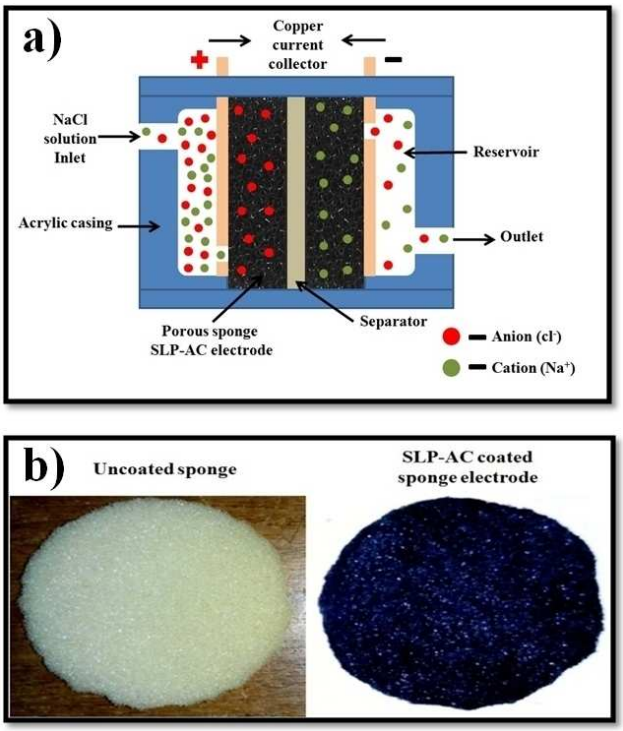

Figure 12. (a) Schematic representation for the flow-through electrode CDI setup (b) SLP-AC uncoated (left) and coated (right) sponge electrode.

Further, we prepared the sponge electrodes (Figure 12b) to study the electrosorption performance of SLP-AC in the as-fabricated flow-through electrode CDI cell. To prepare the sponge electrodes, initially, SLP-AC and sodium dodecyl sulfate

(SDS) were dispersed in DI water with the concentration of 5 mg/mL and 2.5 mg/mL respectively. The solution was kept in a bath sonicator for 2 hours at room temperature to get the homogeneous mixture. Macroporous domestic sponges were cut into circular shape according to the size of CDI setup (approx. size: 5.5 cm diameter X 0.5 cm thickness). To remove the impurities, sponges were cleaned with the DI water and acetone several times in bath sonicator and dried in an oven for 2 hours at 100°C. Cleaned sponges were further dipped into the SLP-AC ink followed by drying for 2 hours at 100°C in air. The dipping and drying procedure was repeated 2 to 3 times in order to get the even coating. Amount of loading should be optimized because less coating affects the conductivity of the resulting SLP-AC sponges; whereas,excess coating closes the pores of sponge and resists the transfer of electrolyte ions. After coating and drying, the sponges were again washed with abundant amount of DI water to remove the surfactant (SDS) and loosely attached SLP-AC, followed by drying in an oven at 100°C for 4 hours to completely remove the water content. The amount of loading was measured gravimetrically. The total amount of SLP-AC loaded onto the sponge electrodes was 60–70 mg. Dried SLP-AC sponges were then used as electrodes in flow-through electrode CDI cell for desalination. Electrosorption performance of the sponge electrodes were analyzed by monitoring the conductivity of salt solution flowing through CDI cell at the specific time intervals. Following equation (9) was used to calculate the electrosorption capacity in mg/g.[47]

$$Electrosorption\ capacity = \frac{(C_o - C_e) \times V}{m} \quad (9)$$

Where, C_o and C_e are the initial and final concentrations (mg/L), V is the volume of NaCl solution (ml) and m is the total mass of SLP-AC loaded on both the electrodes (mg).

Electrosorption analysis using flow-through electrode CDI cell

As discussed earlier CDI system follows the same working principle as electric double layer capacitor (EDLC). The electrochemical characterization of SLP-AC for CDI application was investigated using CV and GCD in 1 M NaCl electrolyte solution (Figure 13). CV profiles were recorded at the scan rates from 50 to 350 mV/s in the potential window of 0 to 0.9 V. Figure 13a shows CV curves without any visible redox peak during charging or discharging, demonstrating the dominance of EDLC due to coulombic interactions; However, the CV curves are not perfectly rectangular may be due to the little involvement of faradic capacitance. Even though we cannot deny the contribution of faradic processes but obtained distinctive symmetrical GCD and CV curves confirms the supremacy of electric double layer and the accumulation of electrolyte ions on electrodes surface are majorly due to the formation of EDL. Certainly, the triangular shape of GCD curves maintained even at the higher current densities displaying the fast movement of salt ions on to SLP-AC electrodes. This confirmed the SLP-AC is an ideal material to carry out the CDI experiments for the removal of salt (NaCl) ions. The specific capacitance obtained for SLP-AC electrodes in 1 M NaCl electrolyte was calculated from the GCD curves using equations (2) and (3). Obtained values at different current densities are 187.97, 178.23, 170.37, 164.61, 159.61, and 153.16 F/g at 1, 1.5, 2, 2.5, 3 and 3.5 A/g respectively (Figure 13c). This higher values of specific capacitance can be attributed to the high surface area and excellent porosity of SLP-AC. These properties are also expected to enhance electrosorption performance.

Applied voltage and the initial concentration of salt solution are the important parameters in the CDI experiment that affects the electrosorption capacity. Hence, to investigate the performance of SLP-AC sponge electrodes in a flow-through electrode CDI cell, we performed the experiment at various voltages and NaCl concentrations in a continuous flow set-up. 50 ml of salt solution was used for all CDI experiments and the flow rate of the solution was kept constant at 10 ml/min using the peristaltic pump.

The procedure for the experiment is as follows; the CDI cell was prepared by inserting the current collectors, electrodes and separator inside the acrylic casing. Complete CDI cell was sealed with the gaskets and stainless steel bolts to avoid the water leakage. Initially, DI water was allowed to pass through the CDI cell for 15 minutes to completely wet the electrodes. After that, the salt solution of known concentration and conductivity was allowed to flow-through the cell without applying any potential difference to tare the physical adsorption. Due to the physical adsorption of ions, the conductivity of the salt solution started to decrease and then remained constant after 10–15 minutes. At that time potential was applied to observe the electrosorption phenomenon. As the potential applied, the conductivity of the salt solution again started to decrease sharply. This was the indication for the successful electrosorption of NaCl ions onto the electrode surface. The decrease in conductivity of salt solution was noted after every 10 minute time interval. The conductivity reduction was observed with time and no significant difference was observed after 90–100 minutes due to the saturation of the electrodes (Figure S2 in the supporting information). The typical electrosorption studies were examined until the conductivity of the corresponding salt solution reaches to equilibrium. Subsequently, when applied potential was reversed; the conductivity of the solution regained its initial value due to the regeneration of electrodes. Regeneration is simply a cleaning process for the electrodes; where adsorbed salt ions can be removed by applying the reverse potential and electrodes can further be reused multiple times for water desalination.

Calibration curve plotted prior to the CDI experiments was used to find out the unknown concentrations from conductivity readings and further used to calculate the electrosorption capacity using equation (9). Figure 14 shows the electrosorption capacities of SLP-AC sponge electrodes under various experimental conditions. As can be seen from the graphs, as the cell voltage increased, the electrosorption capacity also increases and in the case of voltage variations, the electrosorption capacity increases with increasing NaCl concentrations. When compared with the salt removal data obtained

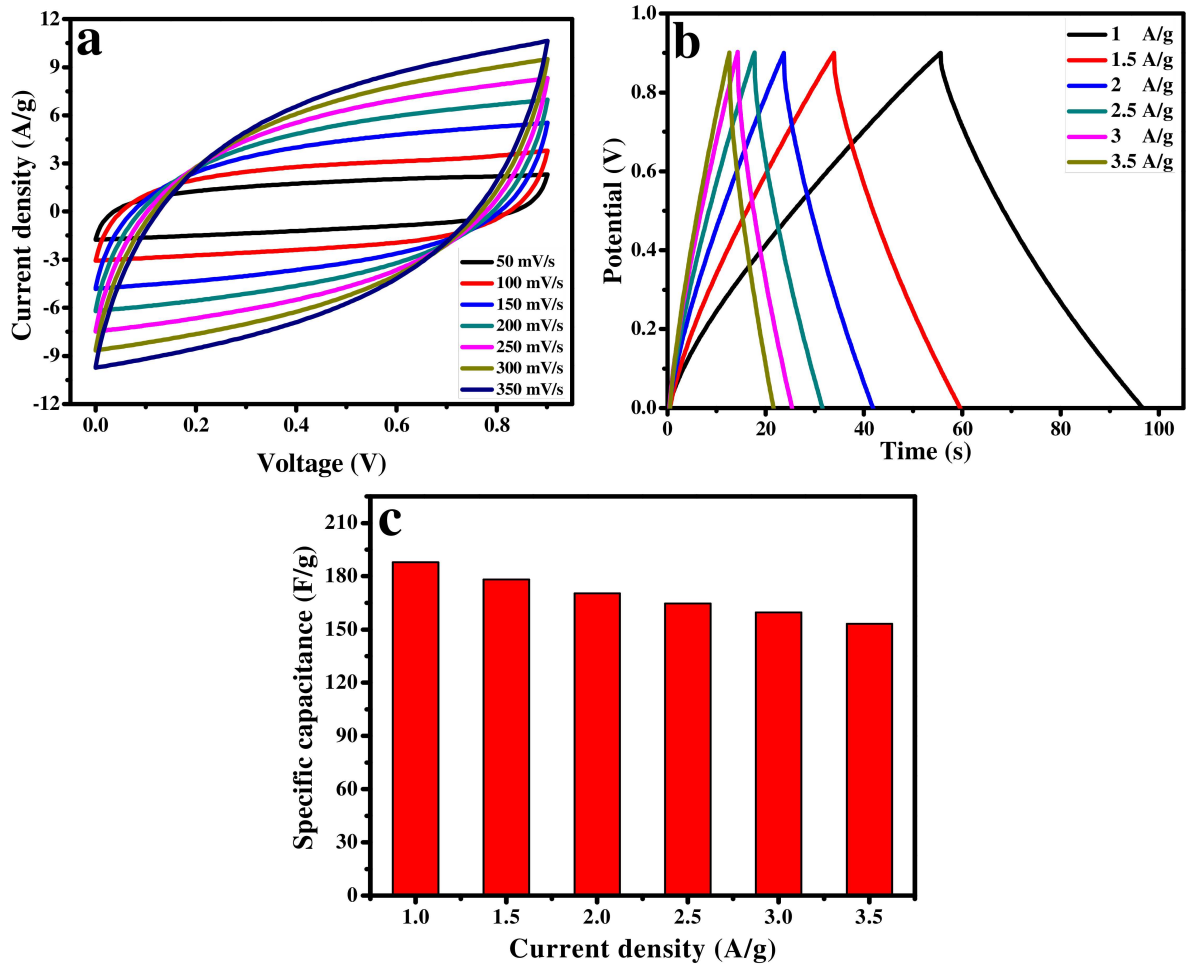

Figure 13. Electrochemical analysis for SLP-AC using two electrode symmetric cell configuration (in 1 M NaCl electrolyte) (a) Cyclic voltammetry at scan rates from 50 to 350 mV/s (b) Galvanostatic charge-discharge at the current densities from 1 to 3.5 A/g (c) Specific capacitance versus current density plot.

from the 300 mg/L of concentration, the electrosorption for 900 mg/L was increased by 68.30%. This is due to the higher mass transfer rate of salt ions within the pores and reduced overlapping effects by an increased concentration of the salt solution.[48] Another possible reason for this is the decrease in electrolyte resistance.[49] The maximum electrosorption capacity was achieved at 1.4 V. However, the performance of SLP-AC was considerably admirable even at low voltage like 0.8 V, confirming the ideal behavior of SLP-AC sponge electrodes for CDI application. In this study, the enhanced electrosorption was largely ascribed to the following reasons; 1) Outstanding wettability of SLP-AC with a water contact angle of 22°; 2) High porosity of activated carbon sponge electrodes; 3) Use of efficient flow-through electrode CDI cell. The salt removal capacity obtained here is the highest compared to the literatures mentioned in Table S4 in the supporting information.

Electrosorption isotherm

Langmuir isotherm

Isotherms have been extensively taken into the considerations to examine the adsorption data, to estimate the adsorption mechanism, and adsorption capacity of the electrode materials. Here, to thoroughly understand the electrosorption of NaCl ions on to the SLP-AC electrodes, we carried out the CDI experiments at different salt solution concentrations (300 mg/L, 600 mg/L and 900 mg/L) and range of applied voltages (0.8 V, 1 V, 1.2 V and 1.4 V). All the obtained experimental data was further used to study the Langmuir (equation 10) and Freundlich isotherm (equation 11).[29]

The Langmuir isotherm representation is suitable only for the surface adsorptions with the limited number of similar sorption sites. The equilibrium data were fitted with this isotherm and can be written as in the form of the following equation.

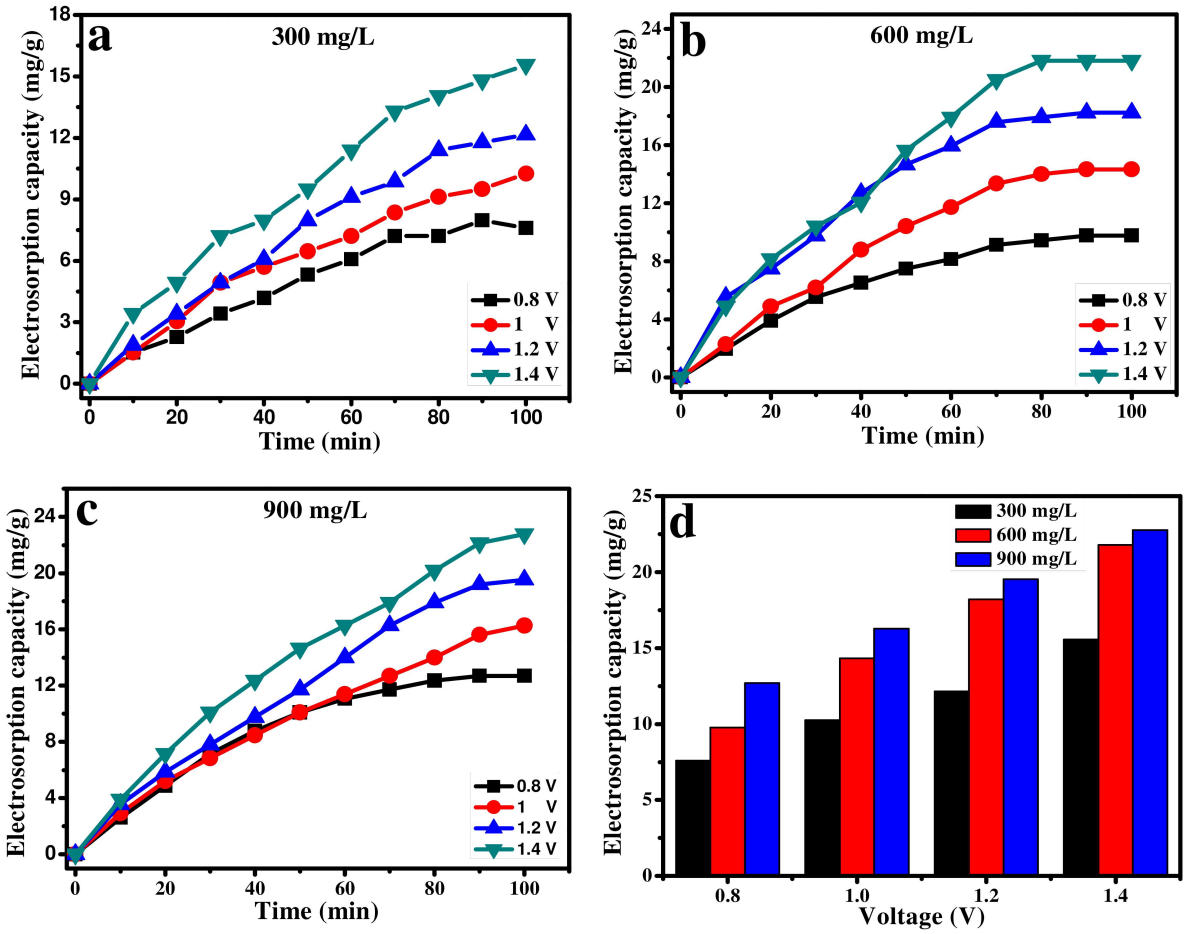

Figure 14. Normalized electrosorption capacity versus time profile at the range of voltages (0.8, 1. 1.2 and 1.4 V) and various concentrations; a) 300 mg/L b) 600 mg/L c) 900 mg/L d) Electrosorption capacity obtained at different applied voltages and concentrations

$$q_e = \frac{q_m K_L C_e}{1 + K_L C_e} \quad (10)$$

Where, q_e is the amount of adsorbed NaCl at equilibrium (mg/g), q_m is the maximum electrosorption capacity (mg/g), C_e is equilibrium concentration of the salt solution (mg/L), and K_L is the Langmuir constant (L/mg).

The equation for the Freundlich isotherm can be written as.

$$q_e = K_F C_e^{1/n} \quad (11)$$

Where, K_f is the Freundlich constant associated with the adsorption capacity of adsorbent and 1/n is the tendency of the adsorbate to be adsorbed.

Figure 15 and S3 in the supporting information demonstrates the fit for the Langmuir and Freundlich isotherm respectively, for the equilibrium electrosorption of NaCl ions onto the SLP-AC sponge electrodes. Additional parameters obtained here are calculated from the intercept and slope for both the isotherms are tabulated in Table 1 and S1 in the supporting information. The correlation factor (R^2) for Langmuir

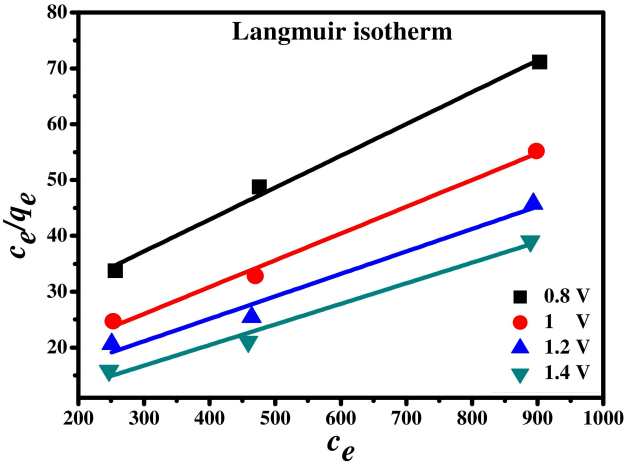

Figure 15. Langmuir isotherm fit for SLP-AC sponge electrodes at various applied voltages for equilibrium NaCl adsorption.

model is closer to 1 compared to that of Freundlich model; confirming the monolayer adsorption of salt ions onto the electrode surface. Hence, the electrosorption of NaCl ions on

Table 1. Parameters obtained from Langmuir isotherm for SLP-AC sponge electrode at different voltages.

Voltages	R^2	q_m	K_L	R_L
0.8	0.999	17.543	0.00284	0.7235
1	0.9882	20.876	0.00411	0.6431
1.2	0.9553	24.875	0.00444	0.6253
1.4	0.9737	27.100	0.00648	0.5335

the electrode material can be explained more exactly by the Langmuir model. The fit obtained from the Freundlich isotherms deviated a lot from the experimental data, particularly at the higher voltages. As mentioned above, the q_m represents the maximum electrosorption capacity (mg/g). Thus from the obtained values, it is clear that the rate of electrosorption increases with applied voltages. The maximum q_m value obtained from the Langmuir isotherm is 27.1 mg/g at 1.4 V, representing the electrosorption limitations for SLP-AC electrode.

Electrosorption kinetics

In order to understand the electrosorption kinetics in detail, the obtained experimental data was further fitted using equations (12) and (13). Figure 16 and S4 in the supporting information show the pseudo-first-order and pseudo-second-order kinetics fitted electrosorption data which was studied with variable parameters like concentration and voltage.[50]

$$ln\ (q_e - q_t) = ln\ q_e - k_1 t \tag{12}$$

$$\frac{t}{q_t} = \frac{1}{k_2\, q_e{}^2} + \frac{t}{q_e} \tag{13}$$

Where, q_e is the amount of NaCl adsorbed at equilibrium (mg/g), q_t represents the adsorption capacity at time t (mg/g), k_1 (mg/g/min) and k_2 (g/mg/min) are the pseudo-first-order and pseudo-second-order rate constants respectively.

Pseudo-first-order kinetics

The values (R^2, q_e, K_1, and K_2) obtained from pseudo-first-order and pseudo-second-order models are mentioned in Table 2 and S2 in the supporting information, respectively. The

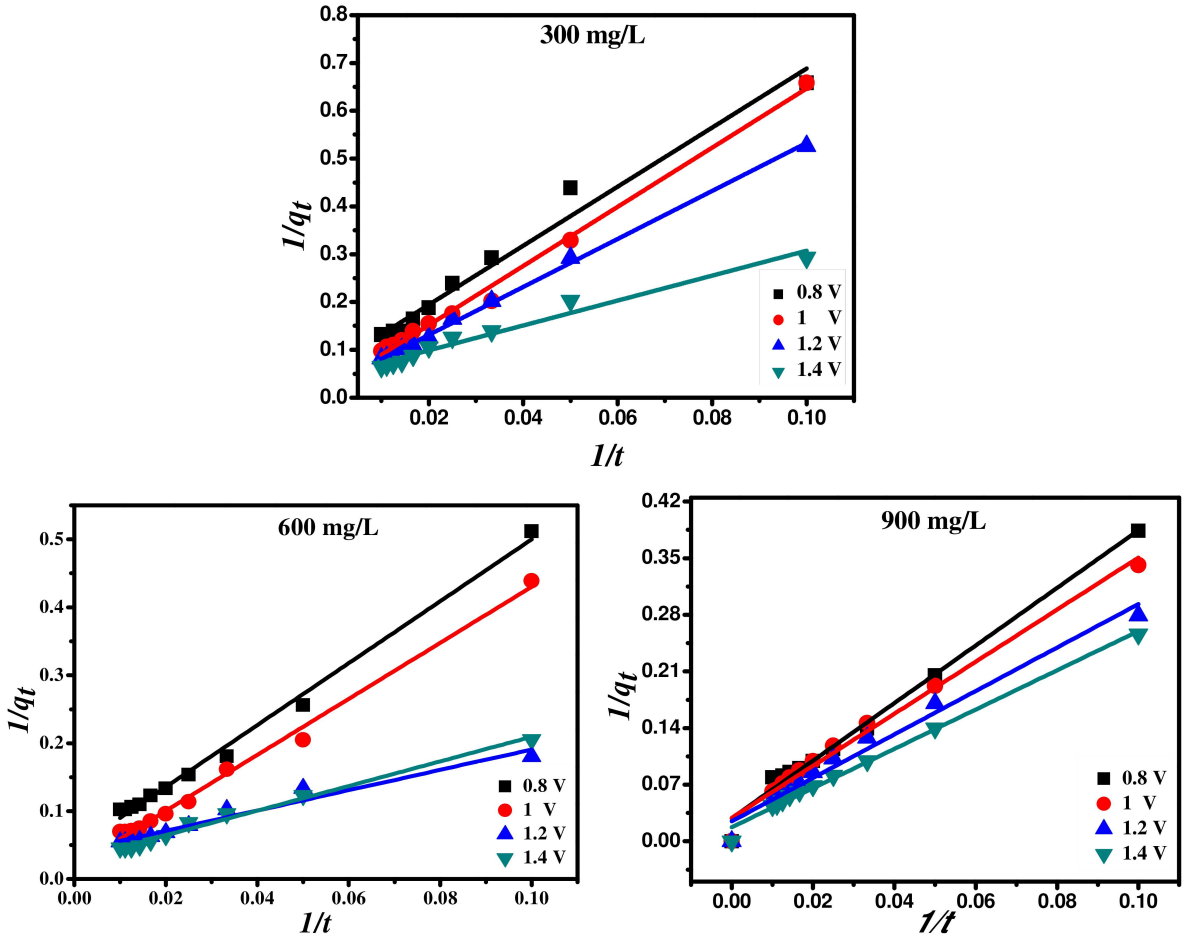

Figure 16. Pseudo-first-order kinetics of SLP-AC sponge electrode for NaCl electrosorption at the range of applied voltages.

Table 2. Electrosorption parameters for pseudo-first-order kinetics at different concentrations and applied voltages.

300 mg/L	R^2	q_e	K_1
0.8 V	0.9893	14.154	1
1 V	0.9972	35.842	1
1.2 V	0.9990	32.552	1
1.4 V	0.9853	21.408	1
600 mg/L	R^2	q_e	K_1
0.8 V	0.9929	22.522	1
1 V	0.9931	56.179	1
1.2 V	0.9568	24.390	1
1.4 V	0.9877	35.460	1
900 mg/L	R^2	q_e	K_1
0.8 V	0.9852	35.714	1
1 V	0.983	35.714	1
1.2 V	0.9744	41.666	1
1.4 V	0.991	58.823	1

correlation coefficient (R^2) for the Pseudo-first-order model is closer to 1 than that of the Pseudo-second-order model, indicating the electrosorption of NaCl onto the SLP-AC electrodes fits well with the pseudo-first-order model. From the data, it is clear that the electrosorption rate is increasing with an applied potential. This can be attributed to the electrostatic forces.[49] The initial concentration of the salt solution also affects the rate of ion adsorption. The rate constants calculated for pseudo-first-order and pseudo-second-order kinetic models are given in detail (Table 2 and S2 in the supporting information). Obtained rate constant values are higher for the pseudo-first-order kinetic model, due to the rapid access of ions into the sponge electrodes through the porous structure.[51]

Conclusion

A facile and low-temperature method has been introduced here for the synthesis of highly porous activated carbon from waste sweet lime peels (SLP-AC). Obtained SLP-AC showed high surface area (667.87 m^2/g) and furtherused to fabricate the electrodes for supercapacitor as well as for capacitive deionization to study its charge storage and electrosorption capacity respectively. SLP-AC demonstrated the highest specific capacitance of 421.67 F/g (at 1 A/g) in aqueous electrolyte and excellent energy density of 45.52 Wh/kg with ionic liquid electrolyte. As prepared SLP-AC electrodes also showed outstanding cyclic stability even after 10000 GCD cycles with a 12% increase in its initial capacitance due to the electroactivation. Electrosorption test performed using SLP-AC sponge electrodes in Flow-through electrode CDI cell resulted in high salt removal capacity of 22.8 mg/g at 1.4 V for 900 mg/L of initial salt solution concentration within 100 minutes. Isotherm studies for electrosorption data fited with the Langmuir isotherm; confirming the monolayer adsorption and kinetics model matched well with the pseudo-first-order kinetics. This easy synthesis technique signifies the potential applicability of SLP-AC as an efficient electrode material for supercapacitor as well as for capacitive deionization applications.

Supporting information summary

Supporting information includes the important information such as Instrumentation, experimental details for the synthesis of SLP-AC, electrochemical characterization i.e. GCD curve for graphitic carbon paper, CV and GCD data for SLP-AC at lower scan rates and higher current densities respectively, CDI data showing change in conductivity with time profile at various voltages and initial salt solution concentrations, Freundlich isotherm, Table for the parameters obtained from Freundlich isotherm, Pseudo-second-order kinetics obtained at various voltages and initial salt solution concentrations, Table for electrosorption parameters obtained from pseudo-second-order kinetics, Comparison table for the energy storage capabilities of activated carbon obtained from various sources, Comparison table for the electrosorption of NaCl by various carbon-based electrodes, and References.

Acknowledgement

The authors would like to acknowledge the financial support from Nanomission programme, Department of Science and Technology, Government of India. (No. SR/NM/NS-1110/2012)

Conflict of Interest

The authors declare no conflict of interest.

Keywords: Activated carbon · Chemical activation · Desalination · Flow-through electrode capacitive deionization · Supercapacitor

[1] A. M. Abioye, F. N. Ani, *J. Teknol.* **2017**, *79*, DOI 10.11113/jt.v79.7249.
[2] L. A. Pfaltzgraff, M. D. Bruyn, E. C. Cooper, V. Budarin, J. H. Clark, *Green Chem.* **2013**, *15*, 307–314.
[3] H. A. Abd El-aal, F. T. Halaweish, *Lucr. Stiintifice Ser. Zooteh. - Univ. Stiinte Agric. Si Med. Vet. Ion Ionescu Brad Rom.* **2010**.
[4] N. R. Kim, Y. S. Yun, M. Y. Song, S. J. Hong, M. Kang, C. Leal, Y. W. Park, H.-J. Jin, *ACS Appl. Mater. Interfaces* **2016**, *8*, 3175–3181.
[5] D. J. Ahirrao, K. Mohanapriya, N. Jha, *Mater. Res. Bull.* **2018**, *108*, 73–82.
[6] W. Qian, F. Sun, Y. Xu, L. Qiu, C. Liu, S. Wang, F. Yan, *Energy Environ. Sci.* **2013**, *7*, 379–386.
[7] A. M. Abioye, F. N. Ani, *Renew. Sustain. Energy Rev.* **2015**, *52*, 1282–1293.
[8] C. Chen, D. Yu, G. Zhao, B. Du, W. Tang, L. Sun, Y. Sun, F. Besenbacher, M. Yu, *Nano Energy* **2016**, *27*, 377–389.
[9] D. Bhattacharjya, J.-S. Yu, *J. Power Sources* **2014**, *262*, 224–231.
[10] L. Wei, K. Tian, X. Zhang, Y. Jin, T. Shi, X. Guo, *ACS Sustain. Chem. Eng.* **2016**, *4*, 6463–6472.
[11] X. Li, W. Xing, S. Zhuo, J. Zhou, F. Li, S.-Z. Qiao, G.-Q. Lu, *Bioresour. Technol.* **2011**, *102*, 1118–1123.
[12] Y. S. Yun, S. Y. Cho, J. Shim, B. H. Kim, S.-J. Chang, S. J. Baek, Y. S. Huh, Y. Tak, Y. W. Park, S. Park, *Adv. Mater. Deerfield Beach Fla* **2013**, *25*, 1993–1998.
[13] Z. Li, Z. Xu, X. Tan, H. Wang, C. M. B. Holt, T. Stephenson, B. C. Olsen, D. Mitlin, *Energy Environ. Sci.* **2013**, *6*, 871–878.
[14] G. A. Ferrero, A. B. Fuertes, M. Sevilla, *Sci. Rep.* **2015**, *5*, 16618.
[15] R.-J. Mo, Y. Zhao, M. Wu, H.-M. Xiao, S. Kuga, Y. Huang, J.-P. Li, S.-Y. Fu, *RSC Adv.* **2016**, *6*, 59333–59342.

[16] H. Wang, Z. Xu, A. Kohandehghan, Z. Li, K. Cui, X. Tan, T. J. Stephenson, C. K. King'ondu, C. M. B. Holt, B. C. Olsen, *ACS Nano* **2013**, *7*, 5131–5141.
[17] A. M. Abioye, Z. A. Noorden, F. N. Ani, *Electrochim. Acta* **2017**, *225*, 493–502.
[18] M. Wahid, G. Parte, D. Phase, S. Ogale, *J. Mater. Chem. A* **2014**, *3*, 1208–1215.
[19] Z. Li, L. Zhang, B. S. Amirkhiz, X. Tan, Z. Xu, H. Wang, B. C. Olsen, C. M. B. Holt, D. Mitlin, *Adv. Energy Mater.* **2012**, *2*, 431–437.
[20] T. E. Rufford, D. Hulicova-Jurcakova, Z. Zhu, G. Q. Lu, *Electrochem. Commun.* **2008**, *10*, 1594–1597.
[21] S. Porada, L. Borchardt, M. Oschatz, M. Bryjak, J. S. Atchison, K. J. Keesman, S. Kaskel, P. M. Biesheuvel, V. Presser, *Energy Environ. Sci.* **2013**, *6*, 3700–3712.
[22] C. Kim, P. Srimuk, J. Lee, S. Fleischmann, M. Aslan, V. Presser, *Carbon* **2017**, *122*, 329–335.
[23] C.-L. Yeh, H.-C. Hsi, K.-C. Li, C.-H. Hou, *Desalination* **2015**, *367*, 60–68.
[24] M. K. , D. J. Ahirrao, N. Jha, *AIP Conf. Proc.* **2018**, *1942*, 050128.
[25] Z. Xie, W. Guan, F. Ji, Z. Song, Y. Zhao, "Production of Biologically Activated Carbon from Orange Peel and Landfill Leachate Subsequent Treatment Technology," can be found under https://www.hindawi.com/journals/jchem/2014/491912/, **2014**.
[26] X. Xu, W. Song, D. Huang, B. Gao, Y. Sun, Q. Yue, K. Fu, *Colloids Surf. Physicochem. Eng. Asp.* **2015**, *476*, 68–75.
[27] Y. Li, Y. Yu, H. San, Q. Han, L. An, *J. Mater. Sci. Chem. Eng.* **2015**, *03*, 9.
[28] N. Shimodaira, A. Masui, *J. Appl. Phys.* **2002**, *92*, 902–909.
[29] X. Xu, L. Pan, Y. Liu, T. Lu, Z. Sun, D. H. C. Chua, *Sci. Rep.* **2015**, *5*, 8458.
[30] H. Yu, W. Zhang, T. Li, L. Zhi, L. Dang, Z. Liu, Z. Lei, *RSC Adv.* **2017**, *7*, 1067–1074.
[31] S. P. Lonkar, V. V. Pillai, S. M. Alhassan, *Sci. Rep.* **2018**, *8*, 13401.
[32] P. H. Wadekar, D. J. Ahirrao, R. V. Khose, D. A. Pethsangave, N. Jha, S. Some, *ChemistrySelect* **2018**, *3*, 5630–5638.
[33] Y. J. Oh, J. J. Yoo, Y. I. Kim, J. K. Yoon, H. N. Yoon, J.-H. Kim, S. B. Park, *Electrochim. Acta* **2014**, *116*, 118–128.
[34] M. S. Balathanigaimani, W.-G. Shim, C. Kim, J.-W. Lee, H. Moon, *Surf. Interface Anal.* **2009**, *41*, 484–488.
[35] H. Wang, D. Zhang, T. Yan, X. Wen, J. Zhang, L. Shi, Q. Zhong, *J. Mater. Chem. A* **2013**, *1*, 11778–11789.
[36] Z.-S. Wu, Y. Sun, Y.-Z. Tan, S. Yang, X. Feng, K. Müllen, *J. Am. Chem. Soc.* **2012**, *134*, 19532–19535.
[37] L. Han, K. G. Karthikeyan, M. A. Anderson, K. B. Gregory, *J. Colloid Interface Sci.* **2014**, *430*, 93–99.
[38] D. Sun, X. Yan, J. Lang, Q. Xue, *J. Power Sources* **2013**, *222*, 52–58.
[39] Q. Cheng, J. Tang, J. Ma, H. Zhang, N. Shinya, L.-C. Qin, *Carbon* **2011**, *49*, 2917–2925.
[40] Y. Chen, X. Zhang, D. Zhang, P. Yu, Y. Ma, *Carbon* **2011**, *49*, 573–580.
[41] W. Liu, X. Yan, J. Lang, Q. Xue, *J. Mater. Chem.* **2012**, *22*, 8853–8861.
[42] X. Zhao, C. Johnston, P. S. Grant, *J. Mater. Chem.* **2009**, *19*, 8755–8760.
[43] M. Biswal, A. Banerjee, M. Deo, S. Ogale, *Energy Environ. Sci.* **2013**, *6*, 1249–1259.
[44] W. Wang, S. Guo, I. Lee, K. Ahmed, J. Zhong, Z. Favors, F. Zaera, M. Ozkan, C. S. Ozkan, *Sci. Rep.* **2014**, *4*, 4452.
[45] C. Falco, J. M. Sieben, N. Brun, M. Sevilla, T. van der Mauelen, E. Morallón, D. Cazorla-Amorós, M.-M. Titirici, *ChemSusChem* **2013**, *6*, 374–382.
[46] L. Jiang, L. Sheng, C. Long, Z. Fan, *Nano Energy* **2015**, *11*, 471–480.
[47] Y. Liu, T. Chen, T. Lu, Z. Sun, D. H. C. Chua, L. Pan, *Electrochimica Acta* **2015**, *158*, 403–409.
[48] Z.-H. Huang, M. Wang, L. Wang, F. Kang, *Langmuir* **2012**, *28*, 5079–5084.
[49] Z. Chen, C. Song, X. Sun, H. Guo, G. Zhu, *Desalination* **2011**, *267*, 239–243.
[50] K. Li, D. Guo, F. Lin, Y. Wei, W. Liu, Y. Kong, *Electrochim. Acta* **2015**, *166*, 47–53.
[51] Y. Gao, L. Pan, H. Li, Y. Zhang, Z. Zhang, Y. Chen, Z. Sun, *Thin Solid Films* **2009**, *517*, 1616–1619.

Submitted: November 1, 2018
Accepted: February 13, 2019